



Earth's Future

RESEARCH ARTICLE

10.1029/2020EF001795

Key Points:

- More than half of the structures in the conterminous United States are exposed to potentially devastating natural hazards
- Growth rates in hazard hotspots exceed the national trend
- Risk assessments can be improved by considering multiple hazards, mitigation history and fine-scale data on the built environment

Supporting Information:

Supporting Information may be found in the online version of this article.

Correspondence to:

V. Iglesias and A. E. Braswell,
virginia.iglesias@colorado.edu;
a.braswell@ufl.edu

Citation:

Iglesias, V., Braswell, A. E., Rossi, M. W., Joseph, M. B., McShane, C., Cattau, M., et al. (2021). Risky development: Increasing exposure to natural hazards in the United States. *Earth's Future*, 9, e2020EF001795. <https://doi.org/10.1029/2020EF001795>

Received 2 SEP 2020

Accepted 2 JUN 2021

Risky Development: Increasing Exposure to Natural Hazards in the United States

Virginia Iglesias¹ , Anna E. Braswell¹ , Matthew W. Rossi¹ , Maxwell B. Joseph¹ , Caitlin McShane², Megan Cattau³, Michael J. Koontz¹, Joe McGlinchy¹, R. Chelsea Nagy¹ , Jennifer Balch^{1,2} , Stefan Leyk¹, and William R. Travis^{1,2}

¹Earth Lab, Cooperative Institute for Research in Environmental Sciences (CIRES), University of Colorado, Boulder, CO, USA, ²Department of Geography, University of Colorado, Boulder, CO, USA, ³Human-Environment Systems, Boise State University, Boise, ID, USA

Abstract Losses from natural hazards are escalating dramatically, with more properties and critical infrastructure affected each year. Although the magnitude, intensity, and/or frequency of certain hazards has increased, development contributes to this unsustainable trend, as disasters emerge when natural disturbances meet vulnerable assets and populations. To diagnose development patterns leading to increased exposure in the conterminous United States (CONUS), we identified earthquake, flood, hurricane, tornado, and wildfire hazard hotspots, and overlaid them with land use information from the Historical Settlement Data Compilation data set. Our results show that 57% of structures (homes, schools, hospitals, office buildings, etc.) are located in hazard hotspots, which represent only a third of CONUS area, and ~1.5 million buildings lie in hotspots for two or more hazards. These critical levels of exposure are the legacy of decades of sustained growth and point to our inability, lack of knowledge, or unwillingness to limit development in hazardous zones. Development in these areas is still growing more rapidly than the baseline rates for the nation, portending larger future losses even if the effects of climate change are not considered.

1. Introduction

Natural hazards, that is, the physical events that cause severe damage or loss (IPCC, 2007), pose an increasing threat to health, safety, property, and critical infrastructure (Cutter & Emrich, 2005; Gall et al., 2011; White et al., 2001). In the United States alone, over 927 billion USD and 32,366 human lives were lost to natural disasters between 1960 and 2015 (CEMHS, 2019). This unsustainable trend is partly attributed to changes in the frequency and magnitude of weather and climate extremes (Batibeniz et al., 2020; Herring et al., 2020). However, historical data for some hazards indicate that escalating losses stem largely from greater exposure due to development in hazard zones (Downton et al., 2005; Gall et al., 2011; Weinkle et al., 2018), despite efforts to reduce impacts with improved hazard mapping, prediction, warning systems, and physical protections. Global assessments yield mixed findings, with some studies showing losses proportional to changes in exposure (e.g., Schumacher & Strobl, 2011), and others identifying declines in loss per unit of exposure starting in the 2010's (e.g., Formetta & Feyen, 2019).

While the terminology varies among hazards researchers and policy-makers, risk is frequently defined as the likelihood of alterations in the functioning of a community resulting from the interaction of hazardous events and social conditions (IPCC, 2012). Risk, or the tendency to incur loss, thus derives from a combination of the physical characteristics of hazardous events (e.g., frequency, magnitude, duration, and areal extent), and exposure, which is a property of social-environmental systems that refers to the presence of people, livelihoods, or social, economic and cultural assets in places that could be adversely affected (Reidmiller et al., 2018). Here, we evaluate how development patterns have changed the exposure of the nation's built environment to natural hazards between 1945 and 2015. We take a historical, multivariate assessment perspective, analyzing occurrence of and exposure to a suite of natural hazards responsible for high damage and fatality rates. To this end, we: (a) build hazard maps of earthquake, wildfire, flood, hurricane, and tornado hazards in the conterminous United States (CONUS), (b) estimate changes in exposure to these hazards using a data set recently created from Zillow (Historical Settlement Data Compilation; HISDAC-US [Leyk & Uhl, 2018; Leyk, Uhl, Connor, et al., 2020; Uhl & Leyk, 2020]), (c) describe the development patterns

that explain changes in exposure, and (d) use a case study from the Sacramento Valley to evaluate how management practices and human modification of natural systems influence risk at the local scale. While this example focuses on the relationship between flood exposure and vulnerable structures, it is intended to highlight more broadly the opportunities that structure-level data provide for hazard risk assessment.

2. Data and Methods

2.1. Building a Geography of Hazards in CONUS

We obtained information on earthquake, wildfire, hurricane, and tornado hazard from federal agencies, and on flood hazard from Fathom. Although the independent data sets are well-suited for empirical risk assessments, evaluations across multiple hazards remain problematic. Hazards are measured in terms of frequency or intensity, and on scales specific to each physical process. In addition, data sets may contain empirical observations, modeled potentials or a mixture of both. Different units and data limitations including missingness and varying resolution make combining hazard measures challenging. Here, we detail the hazard layers we used and assumptions made with each data set.

2.1.1. Earthquake

The earthquake hazard layer was obtained from the United States Geological Survey (USGS) Earthquake Hazards Program (Rukstales & Shumway, 2019). The layer depicts peak ground acceleration with a 2% probability of exceedance in 50 years on a uniform firm rock site (shear wave velocity in the upper 30 m of the Earth's crust = $V_{S30} = 760 \text{ m}\cdot\text{s}^{-1}$). The model used to develop the hazard layer incorporates more than 100 years of global earthquake observations, widely accepted seismology-based principles, and a long history of analyses in the science and engineering communities. Inputs to the model are based on regularly updated, time-independent estimates of locations and sizes of future earthquakes (Petersen et al., 2020). Since the data represent a 2% probability of exceedance over 50 years, we set all values below 0.02/50, or 0.0004 annual probability of exceedance, to zero.

2.1.2. Flood

To estimate river flood hazard, we used a 30-m resolution, two-dimensional hydrodynamic model developed by Fathom (Sampson et al., 2015; Wing et al., 2017). This model was produced using publicly available data, including the USGS National Elevation Data set, and validated against Federal Emergency Management Agency (FEMA) Special Flood Hazard Area maps and local hydraulic models from the USGS. Fathom provides the results for two model variants of river flooding at multiple recurrence levels. The first variant is an “undefended” version where levees are not incorporated into the hydrodynamic model. The second variant is a “defended” version where the effect of levees in the US Army Corp of Engineers National Levee Database are included into the hydrodynamic model. We used the “defended,” 100-year flood model for national scale analyses. However, we evaluate the importance of this decision in the case study of the Sacramento Valley (Section 4).

2.1.3. Hurricane

We developed the hurricane hazard layer with modeled wind fields constructed from the Extended Best Track Data set from the Atlantic basin, which contains tropical storms from 1988 to 2015 (Demuth et al., 2006). We only considered hurricanes whose paths came within 250 km of one or more US counties. For each storm, 15-min maximum sustained wind speeds were estimated on a 1° grid using the stormwindmodel R package (Anderson, Ferreri, et al., 2020; Anderson, Schumacher, et al., 2020). We then computed annual maxima from these event-specific fields on a 1° grid and averaged across years for each grid cell. Because wind fields average over several years when there is very low to zero impact from hurricanes, the values that we report should not be interpreted as typical wind speeds during a hurricane (they are much lower). Instead, this spatiotemporally integrated value serves as an indicator of hurricane winds that scales with both the frequency of hurricanes impacting a given grid cell and the historic magnitudes of those events.

2.1.4. Tornado

The tornado hazard layer was based on spatial paths of tornadoes (1950–2018) obtained from National Oceanic and Atmospheric Administration's (NOAA) National Weather Service Storm Prediction Center

severe report database (NOAA, 2019). We subset these paths to exclude tornadoes prior to 1982, when the F-scale rating began to be consistently recorded. Each path was buffered by 300 m, a distance similar to the mean recorded path widths reported in previous studies (Agee & Childs, 2014). To obtain a hazard layer of annual frequency, we rasterized the buffered paths and computed a summary raster layer where the values represented the fraction of years from 1982 to 2018 that each grid cell was exposed to one or more tornadoes. Even though event footprints are small, the weather systems that produce them are meso-scale (tens to hundreds of km) leading to auto-correlation in the historic record that requires smoothing for hazard assessment (Dixon et al., 2013). For this reason, the tornado raster layer was smoothed using a focal mean function with a circular shape of 10-km radius.

2.1.5. Wildfire

We employed the wildfire hazard layer from the wildfire hazard potential (WHP) product developed by the Fire Modeling Institute (Forest Service, United States Department of Agriculture). This data set integrates burn probability and intensity (Short et al., 2016), vegetation data from LANDFIRE 2012 and wildfire occurrence data from the FPA-FOD (Short, 2017) to represent the relative potential for wildfire that would be difficult for suppression resources to contain (Dillon, 2018). Given that WHP depends on vegetation type and continuity, this hazard layer is not independent of urban development.

2.2. Identifying Hazard Hotspots

Hazards were measured at different spatial resolutions and with different units. To compare them and estimate exposure, we resampled all hazard layers to a 250 × 250 m reference grid projected in NAD1984 USGS-Albers-Equal-Area-Conic (Figure S1). Resampling was performed via bilinear interpolation, that is, we computed the value of a cell as a function of the weighted average of the four nearest input cell centers (Gonzalez & Woods, 2002). We then defined hotspots for each natural hazard as grid cells where the probability or intensity of the hazard exceeded the 90th percentile among all grid cells in CONUS. In all cases, percentiles were based on unique hazard values (Figure S2).

2.3. Estimating Changes in the Built Environment Within Hotspots

Exposure is often measured by the number of people physically in harm's way (Schumacher & Strobl, 2011). Alternatively, risk assessments conduct inventories of structures to assess location of people and property in relation to a hazard (Highfield et al., 2014; Fuchs, Keiler, & Zischg, 2015; Fuchs, Röthlisberger, et al., 2017). Settlement patterns and their changes are typically derived through classification of satellite images or maps, which provide information on the location and nature of land use related to the built environment (Ehrlich et al., 2018; Paprotny et al., 2018). However, several data limitations affect efforts to assess hazard exposure and vulnerability. First, remotely sensed data products are constrained to the post-1970 era of satellite technology. Second, they tend to be coarsely classified by development intensity, thus lacking specific characteristics of built-up land. Finally, most of these data products are less accurate for rural areas (Leyk & Uhl, 2018).

To estimate detailed, consistent development patterns (Smith et al., 2002; Wickham et al., 2013), we used the Historical Settlement Data Compilation for the US (HISDAC-US; Leyk & Uhl, 2018; Uhl & Leyk, 2020). HISDAC-US is a collection of gridded settlement layer time series derived from the Zillow Transaction and Assessment Data set (ZTRAX), a housing and property database that contains over 370 million records on housing and land-parcel attributes. Recent work shows a strong correlation between built-up property counts in HISDAC-US and population size (Leyk, Uhl, Connor, et al., 2020), indicating that estimates of exposure based on this data set also serve as an approximation to the number of people in harm's way. We note that issues of missing building records or spatial offsets in geolocations affect ZTRAX data, and are subsequently inherited by HISDAC-US. However, an accuracy assessment with parcel records and building footprints found F-measures of greater than 0.9 for each year of the database (Leyk & Uhl, 2018).

Our analyses are based on a version of the structure count data that is undissolved, meaning that it documents all structures, including multiple units in a building, and does not incorporate agricultural land use. Land use is characterized through description fields in the ZTRAX data set. We employed the attribute

“PropertyLandUseStndCode” to determine land-use types and create gridded time series of development layers. Each record in ZTRAX was assigned a pixel group through grid indexing, which created three attributes for each structure. The three new attributes, x , y , and location ID are linked to and describe the positions of the 250×250 m grid cells projected in NAD1984 USGS-Albers-Equal-Area-Conic. Thus, each built structure is linked to an underlying grid cell or pixel group.

For each point in time, we determined the most frequent land-use code per pixel group and assigned this value to the output template grid at the designated grid ID. While generating time series of the number of properties per grid cell, we registered missing data across multiple attributes. Records that did not have a value for the built year or did not have a value for land use were separated from the database. As this study was generalized across CONUS, local data incompleteness issues should not significantly affect our results.

Finally, we estimated trends in development for 1945–2015 at 5-year intervals by overlaying the development and hazard layers. For each hazard, exposure was calculated as the density of structures within the corresponding hotspot (Equation 1).

$$\text{Exposure}_{(h,t)} = \sum \text{structures}_{(h,t)} \times \text{area}_h^{-1}, \quad (1)$$

where h is a hazard hotspot and t is a year. Area_h was obtained by multiplying the number of grid cells within each hazard hotspot h by the area of a grid cell (250×250 m).

2.4. Describing the Development Patterns That Explain Changes in Exposure

In order to account for regional and historical differences in development in each hazard hotspot, we focused on two distinct components of urbanization: expansion and densification (Leyk, Uhl, Connor, et al., 2020). Expansion refers to the development of formerly undeveloped land, and was calculated as (Equation 2):

$$\text{Expansion}_{(h,t)} = \text{Occ_area}_{(h,t)} \times \text{area}_{(h)}^{-1}, \quad (2)$$

where h is a hazard hotspot, t is a year and occ_area is the surface area of all cells with at least one structure.

Trends in densification, that is, the addition of new structures to previously developed areas, were obtained with Equation 3:

$$\text{Densification}_{(h,t)} = \sum \text{structures}_{(h,t)} \times \text{occ_area}_{(h,t)}^{-1}, \quad (3)$$

where h is a hazard hotspot, t is a year and occ_area is the surface area of all cells with at least one structure.

Temporal trajectories in exposure, expansion and densification were calculated for the total number of structures in each hotspot. The distribution of structures per grid cell ranges from 1 to 9,831 and is heavily skewed. To prevent trajectories from being dominated by the highest-density cells, we grouped structure counts per cell at each point in time into three density classes defined by natural breaks in the data: low density (<113 structures $\times \text{km}^{-2}$), intermediate-density (113–1,130 structures $\times \text{km}^{-2}$), and high-density ($>1,130$ structures $\times \text{km}^{-2}$; See Figure S3 for details). Given the similarities between the mosaic of rural/urbanized areas produced by the US Census Bureau (Ratcliffe et al., 2016) and the spatial distribution of density classes (Figures S1f and S4), we expected that these divisions would serve as an overall approximation to development patterns in rural, suburban/urban and dense metropolitan areas.

We calculated exposure, expansion and densification for each density class in all hotspots according to Equations 1–3, respectively. These equations were slightly modified to estimate national trends, where the parameter area_h (area of the hazard hotspot) was replaced by the surface area of CONUS.

2.5. Informing More Targeted Hazard Risk Analysis: Relationships Among Hazard, Exposure, and Vulnerability at Local Scales

In order to illustrate how our national scale analyses can inform more targeted risk assessment at the local level, we developed a case study of the Sacramento Valley (California) and examined relationships among hazard, protective interventions, exposure, and vulnerability. In particular, we assessed the effects of adaptation (e.g., physical flood defenses) and changes in exposure of the most vulnerable properties. Our approach is in keeping with Federal Emergency Management Agency guidelines for hazard mitigation plans for the Sacramento Valley, an area in a flood hazard hotspot. We focused on floods because this hazard layer allows the explicit quantification of the role of social-technological intervention on development patterns. To this end, we differentiated flood depths in the absence of levees (“undefended” model) against those associated with levees (“defended” model) to determine where and how much flood water is displaced from protected areas to bypasses. Large positive values correspond to defended areas behind levees, and small negative values are indicative of places where water was routed once the defensive structures were installed. With this information, we estimated flood risk as a function of the depth of the 100- and 500-year floods in Hydrologic Unit Code 8 (Steeves & Douglas, 1994) using Equation 4:

$$\text{Risk}_{(\text{flood}, \text{huc8}, t)} = \text{depth}_{(\text{flood}, \text{huc8})} \times \sum \text{structures}_{(\text{huc8}, t)}, \quad (4)$$

where flood is a flood return interval (i.e., 100 and 500 years), huc8 is a Hydrologic Unit Code 8, t is a year, and depth is the water depth. We attributed differences in risk between the defended and undefended models to the inclusion or exclusion of flood control levees.

Finally, we separately calculated the relative proportion of vulnerable to total structures in areas where the differences between flood depths in the undefended and defended models were <-0.5 , -0.5 to 0 , 0 – 0.5 , and >0.5 m. Vulnerable land use refers to unsafe structures, properties with large numbers of inhabitants, and critical/institutional facilities, that is, mobile homes, trailer parks; multi-family dwellings; welfare, social-service, and low-income housing; apartment buildings with more than 100 units; high-rise apartments; boarding and rooming houses; transient lodging; motels; medical buildings, and clinics; private and public hospitals; public-health care facilities, nursing, rest, convalescent, handicap, and retired homes; residential group homes; public schools, and correctional facilities. We selected these groups based on land-use types that were identified in the literature as particularly vulnerable to hazards (Cutter, Boruff, & Shirley, 2003; Ma & Smith, 2020; Petal, 2004; Segal et al., 2017; Wilson et al., 2019).

3. Results and Discussion

3.1. Over Half of Existing Structures Lie Within Hazard Hotspots, and Exposure is Increasing

Natural hazards have unique geographies dictated by complex environmental dynamics (Figure S1). The general relationship between the probability and magnitude of natural events is heavy-tailed and resembles a stretched exponential distribution or a power-law (Figure S2). As a consequence, the probability of extreme events is higher than under the assumption of normality. Given that unusual, very large events reside in the right tail of the frequency-size distribution, we defined hazard hotspots as pixels where event probability or magnitude exceeded the 90th percentile of all unique values in CONUS. Hotspots therefore correspond to the most hazardous subregions of hazard zones used in exposure assessments (e.g., Willis et al., 2016, and references therein). Historically, the most devastating natural disasters, such as the San Francisco earthquake (California; April 1906; $\sim 3,000$ fatalities; ~ 11 billion inflation-adjusted 2019 USD loss), Galveston hurricane (Texas and Oklahoma; September 1900; 6,000–12,000 fatalities; ~ 1 billion inflation-adjusted 2019 USD), and the tri-state tornado (Illinois, Indiana, and Missouri; March 1925; 629 fatalities; ~ 2.3 billion inflation-adjusted 2019 USD) occurred in these hazard hotspots. Recent disasters in New Orleans (Hurricane Katrina), Houston (Tropical Storm Harvey), and New York/New Jersey (Superstorm Sandy) speak to a continuation of this trend.

The combined area of all hazard hotspots covers $\sim 31\%$ of the country (Figure 1a). However, $\sim 57\%$ of structures lie within their boundaries. In 1945, $\sim 173,000$ structures were located in the intersection of at least two hazard hotspots. After seven decades of sustained growth, this number surpassed 1.5 million structures.

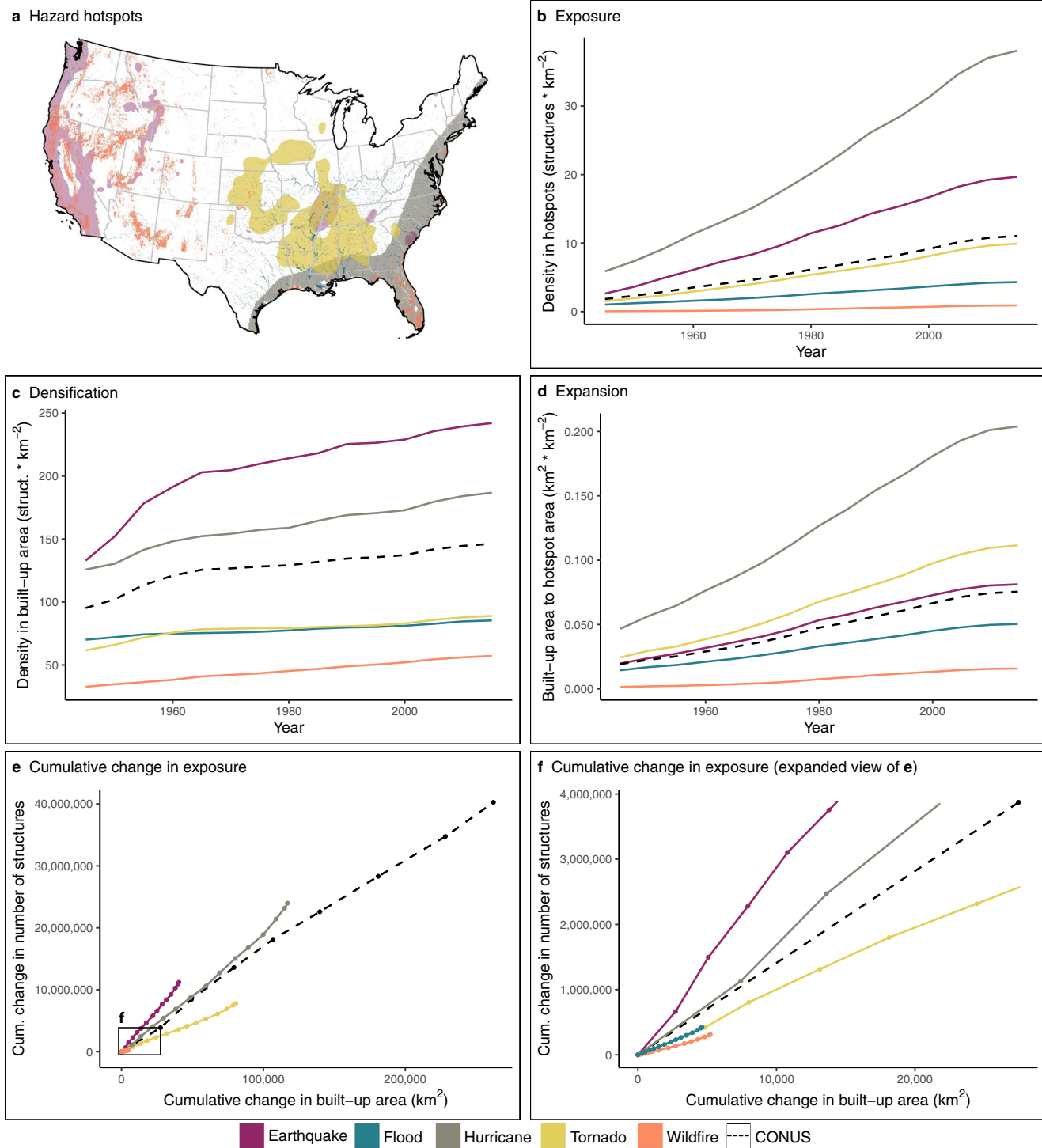


Figure 1. Trends in exposure in hazards hotspots (1945–2015). The probability/magnitude of natural events is assumed to be constant over the entire period, and changes in exposure are attributed solely to development. (a) Location of hazard hotspots (top 10% of unique hazard values). Temporal trends in (b) exposure, (c) densification, and (d) expansion of structures in each hotspot. (e) Cumulative change in the number of structures as a function of cumulative change in built-up area for each hazard. The dots represent years between 1945 and 2015 at 5-year intervals. (f) Expanded view of the area indicated with a rectangle in (e).

These critical levels of exposure point to our inability, lack of knowledge, or unwillingness to limit development in hazardous zones (Cutter & Finch, 2008; Cutter, Hodgson, & Dow, 2001). Rapid increases in building density in a subset of hotspots underlie this pattern (Figures 1b–1f). In particular, the density of structures in earthquake- and hurricane-prone areas increased faster, and is currently higher, than average trends in development for CONUS as a whole (1.7 and 3.1 times higher, respectively). Contrasting development trajectories were observed in the remaining hazard hotspots. Structures were added to tornado-prone areas at rates that closely match the national averages. Trends in structure density in zones coinciding with the wildfire or flood hotspots fall below the national trajectory (Figure 1b). These differences suggest that the observed exposure results from the interaction of unique hazard geographies with the legacy of idiosyncratic long-term development trajectories.

Development trajectories can be decomposed into two distinct processes: Densification (addition of structures to previously developed lands), and expansion into formerly undeveloped areas. In hazard hotspots, densification was initially rapid and decelerated in recent decades (Figure 1c). Frequently, high densification is the product of rapid influx of population and capital to urbanized areas. Conversely, expansion, which is often associated with the addition of less expensive housing, has linearly increased since the 1940's (Figure 1d). Despite relatively similar long-term trends, we find notable differences among hazards in the relative contribution of densification and expansion to total exposure (Figures 1e and 1f). Specifically, development in earthquake and hurricane hotspots was primarily driven by densification, most of which occurred prior to 1960 (Section 3.2). Increases in exposure to wildfires, floods, and tornadoes, in contrast, have mostly taken place in the form of expansion (Section 3.3).

Exposure to natural hazards is a necessary but insufficient determinant of risk, as impacts are also conditioned on the vulnerability of social-environmental systems (Cutter, Boruff, & Shirley, 2003; Emrich & Cutter, 2011; Turner et al., 2003). Adaptive capacity is constrained by social and economic disparities, which are often the by-product of the historical and demographic processes underpinning the mosaic of land uses (Grimm et al., 2008; Smit & Wandel, 2006; Vogel & O'Brien, 2004). National scale assessments that explicitly factor in the relative contribution of expansion and densification to exposure across the urban-rural gradient can therefore help identify social-economic contexts associated with otherwise hidden inequity of vulnerability.

3.2. Increasing Exposure to Earthquakes and Hurricanes is Primarily Driven by Densification of Urban/Suburban Areas

3.2.1. Earthquakes

Seismic hazard maps suggest that large earthquakes are more likely to occur in the western United States (Figure S1a), where earthquake magnitude is largely dictated by regional tectonics and the distribution of stress along major plate boundaries, including the San Andreas transform boundary (California), the Cascadia subduction zone (Pacific Northwest), and the eastern margin of the Basin and Range extensional province (northern Mountain West). In the east, hazard is relatively low except in the proximity of zones of historic intraplate deformation, particularly near the New Madrid Seismic Zone (south-central Mississippi Valley).

The earthquake hotspots defined in this study correspond to an area of 658,000 km² with a 2% probability of peak ground acceleration (PGA) of at least 0.35 g in 50 years. Although the correlation between instrumental scales, such as PGA, and other intensity measures has large uncertainties, the United States Geological Survey (USGS) characterizes the perceived shaking of earthquakes in hotspots as “severe” to “extreme,” and their possible damage as “moderate” to “very heavy” (Worden, 2016). The partition of the HISDAC-US data set into density classes (i.e., low density: 1–112 structures × km⁻²; intermediate-density: 113–1,130 structures × km⁻²; and high-density: >1,130 structures × km⁻²) shows that 90% of the 13 million structures exposed to potentially devastating earthquakes (Figures 2a and 2b), are located in high- and intermediate-density areas. These estimates are heavily weighted by structure densities in urban-suburban cores along the Pacific coast (e.g., Seattle, Portland, San Francisco, and Los Angeles) and some isolated cities in the central to southeastern US (e.g., Charleston, Memphis, and Knoxville). In these metropolitan areas,

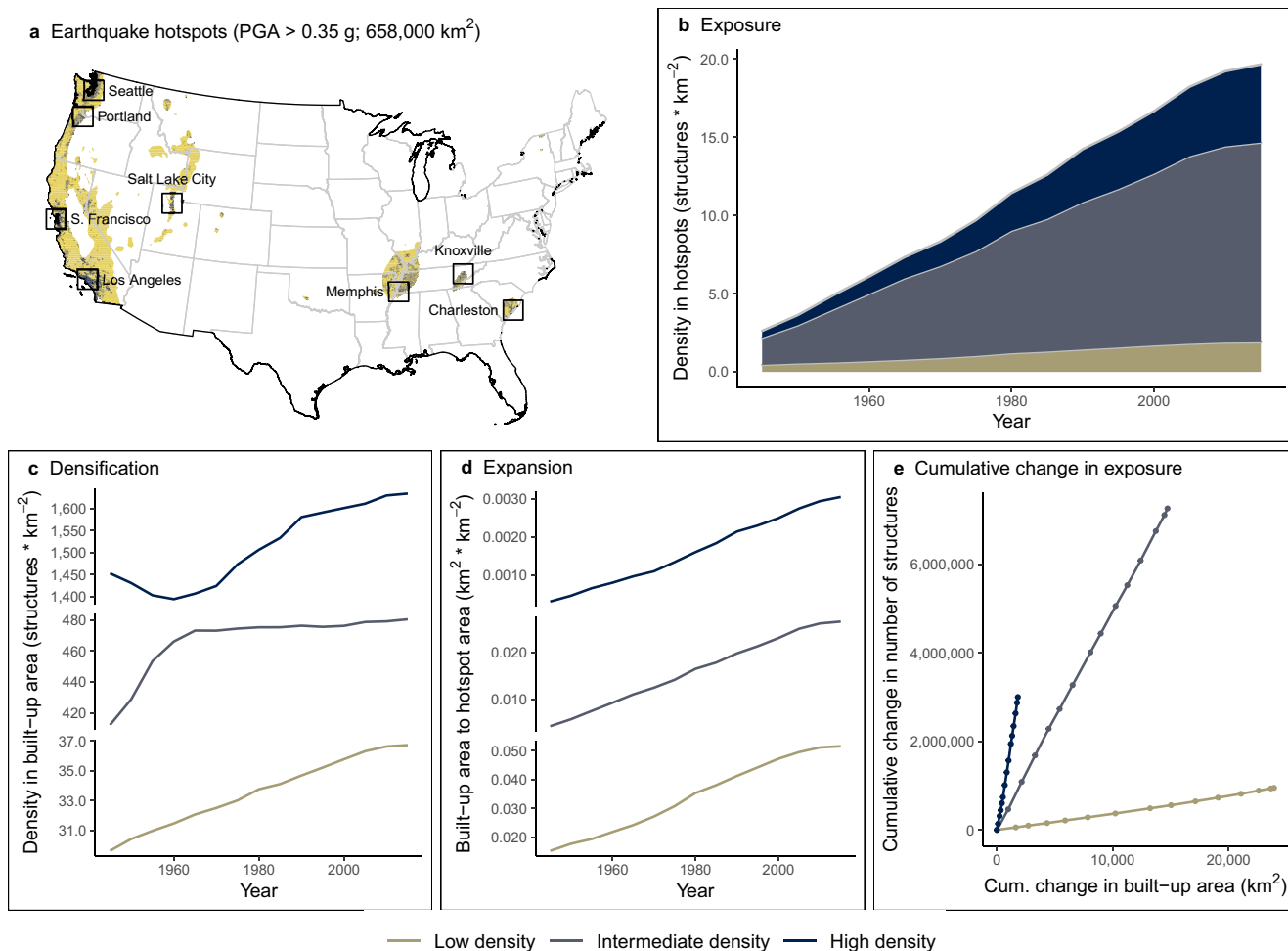


Figure 2. Exposure to earthquakes (1945–2015). Peak ground acceleration (PGA) is assumed to be constant for the entire period, and changes in exposure are attributed solely to development. (a) Location of the earthquake hotspots. Temporal trends in (b) exposure, (c) densification, and (d) expansion of structures in the earthquake hotspots. Note that y-axis scales are different in (c and d). (e) Cumulative changes in the number of structures in the earthquake hotspots as a function of cumulative changes in occupied area. The dots represent years between 1945 and 2015 at 5-year intervals. In all cases, the variables are grouped by classes of development density (i.e., low density = 1–112 structures × km⁻²; intermediate-density = 113–1,130 structures × km⁻²; and high-density >1,130 structures × km⁻²).

high probability of ground motion coupled with great potential for damage result in high seismic risk, with Los Angeles County alone accounting for 22% of the annualized loss from earthquakes nationwide (Jaiswal et al., 2017).

Between 1945 and 2015, the number of structures in major seismic areas increased monotonically and was consistently higher than the national trends (Figures 1b and 2b). We attribute this trajectory to the continuous addition of new buildings to already dense areas, along with sustained but local expansion into undeveloped lands (Figures 2b–2e). Prior to 1965, periods of slower densification in high-density regions coincide with rapid development of intermediate-density zones. This trade-off is consistent with fast growth of cities often observed in coastal states (Crossett et al., 2005; Hauer et al., 2016), and exemplifies the interdependence of densification and expansion, as densification frequently leads to outward expansion due to a variety of complex social, economic and cultural factors (e.g., people being priced out of urban centers). Given the right conditions, these newly developed lands may become high-density areas in time.

As the number of structures rises, so do the capital and human lives exposed to potentially devastating events. However, greater exposure does not necessarily imply a proportional increase in seismic risk. Building codes and construction standards for earthquake resistance are constantly improving, meaning that

modern structures are likely to be less vulnerable than aging buildings, and retrofitting can reduce potential damage (ASCE, 2014). Losses from earthquakes, nonetheless, continue to increase in CONUS and worldwide mainly because development outpaces hazard mitigation (Jaiswal et al., 2017; Lyles et al., 2014; Tucker, 2007).

3.2.2. Hurricanes

Hurricanes primarily affect the eastern half of CONUS, with the highest number of occurrences along the Atlantic and Gulf Coast states (Figure S1c). The majority of hurricanes occur between June and November, driven by seasonal thermodynamics, particularly those related to changes in sea-surface temperature and vertical wind shear over the Atlantic (Latif et al., 2007). Hurricanes cause extreme wind, storm surge, rain, and flooding, all of which can lead to substantial damage and loss of lives (Rappaport, 2014; Weinkle et al., 2018; Willoughby, 2012).

Hurricane Harvey illustrates this phenomenon (Figure S5). In August 2017, Category 4 Hurricane Harvey made landfall in Texas, with 52 associated tornado events, record amounts of precipitation, and extensive flooding exacerbated by anthropogenic climate change and urbanization (Risser & Wehner, 2017). The losses of the Harvey-associated tornadoes were over 7 million USD (SVRGIS, 2019). In addition, 6.8 billion USD was paid out across over 75,000 building-related flood insurance claims, along with more than 2 billion USD over 52,000 contents-related insurance claims (FEMA NFIP, 2020). Unlike the capital losses to compound disturbances, the combined effects of multiple hazards may be non-additive. For example, tornado warnings advised people to “seek shelter in an interior room on the lowest floor” of their homes, many of which were flooded (Evans, 2018). Conflicting actions to mitigate risk from multiple hazards thus introduce additional challenges, including overcrowding in evacuation centers with increased disease risk.

Here, we focus on wind gusts resulting from hurricane events. Associated rain and flooding show similar spatial patterns, albeit marked by a somewhat broader spatial domain (Zhou & Matyas, 2017). The area subject to the top 10% average maximum wind fields, hereafter hurricane hotspots, occurs across 744,500 km² of the intensely developed Atlantic and Gulf coasts (average maximum wind speed >6 m·s⁻¹; Figure 3a). Mainly as a consequence of the densification of coastal cities, including Houston, Miami, Boston, and New York, at least 28 million structures are exposed to strong winds from Atlantic tropical storms. In contrast to the earthquake hotspots (Figure 2), more sustained increases in expansion occurred over all three density classes and accompanied the densification process (Figures 3b–3e). Differences in the relative role of expansion in these hotspots likely arise from underlying environmental, social and political conditions. Suburban structures have expanded more in the less-fragmented landscapes of the East, particularly across the coastal plains. Conversely, restrictive land-use policies, geographic and topographic limitations, and escalating housing costs have constrained the expansion of urban cores on the West Coast (Alig et al., 2004; Boschken, 1982).

Urbanization, rather than climate change, has been identified as the main cause of increasing losses to natural hazards in metropolitan areas across the US (Bouwer, 2011; Depietri & McPhearson, 2018). Urban cores are home to a large proportion of the nation’s population and assets, and function as administrative, economic and innovation centers. As a result, the direct impacts of natural hazards in these areas can be severe and trigger cascading impacts that extend beyond city limits (Godschalk, 2003; Sebastian et al., 2007). The indirect consequences, including supply-chain and business interruption, unemployment, and relocation of potentially large numbers of individuals, also have long-term effects that are distributed unequally across socioeconomic populations (Davies et al., 2018; Emrich & Cutter, 2011).

Demographic studies reveal that resources tend to increase after major hurricanes while poverty levels do not change significantly (Pais & Elliott, 2008). These contrasting trends reflect post-disaster socioeconomic polarization, which is frequently associated with the proliferation of smaller, wealthy neighborhoods in severely damaged urban areas along with the displacement of racial minorities (Schultz & Elliott, 2013). However, comparison of post-Hurricane Andrew demographic trajectories in Miami, Florida, and less-populated areas of Louisiana suggests that displacement of disadvantaged groups prevailed in urban areas but the contrary was observed in more rural settings. There, vulnerable groups were unable to relocate whereas more advantaged residents moved and, in cases, upgraded their residential circumstances (Elliott & Pais, 2010). Differential impacts and post-disaster recovery trends across the rural-urban spectrum

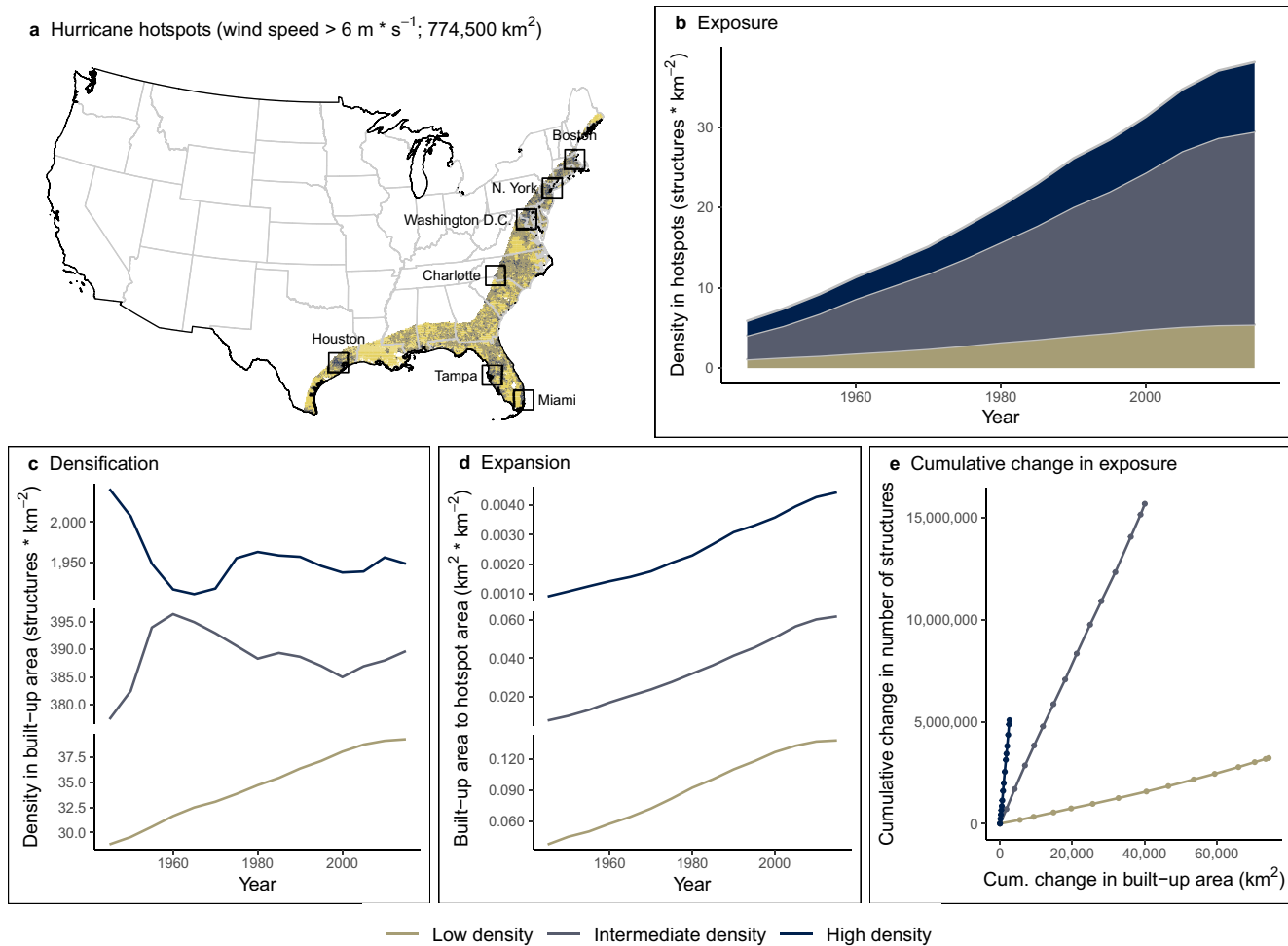


Figure 3. Exposure to hurricanes (1945–2015). Hurricane probability is assumed to be constant over the entire period, and changes in exposure are attributed solely to development. (a) Location of hurricane hotspots. Temporal trends in (b) exposure, (c) densification, and (d) expansion of structures in the hurricane hotspots. Note that y-axis scales are different in (c and d). (e) Cumulative changes in the number of structures in the hazard hotspots as a function of cumulative changes in occupied area. The dots represent years between 1945 and 2015 at 5-year intervals. In all cases, the variables are grouped by classes of development (i.e., low density = 1–112 structures × km⁻²; intermediate-density = 113–1,130 structures × km⁻²; and high-density >1,130 structures × km⁻²).

highlight the need to incorporate high-resolution structure and population data such as HISDAC-US in exposure and risk assessments.

3.3. Increasing Exposure to Floods, Tornadoes, and Wildfires is Primarily Driven by Expansion of Suburban and Rural Development

3.3.1. Floods

Flood hazard is widespread, but highest near river channels with large contributing drainage areas (e.g., Mississippi River and its tributaries) and broad floodplains (Figure S1b). The location and timing of the largest flows vary geographically, reflecting differences in rainfall magnitude, antecedent conditions, and/or snowmelt dynamics (O'Connor & Costa, 2004). Interacting climate, geology, management, sediment dynamics, and dominant runoff generation mechanisms result in large unit discharge in places like southern Texas, the western slopes of the Cascade Range, and throughout the Appalachians.

The flood hazard hotspots defined in this study are constrained to floodplains where the water depth of the 100-year flood exceeds 0.6 m (i.e., 90th percentile flood depth). We focused on 100-year events because that is the parameter used by FEMA for floodplain management and insurance regulations (See Section 4

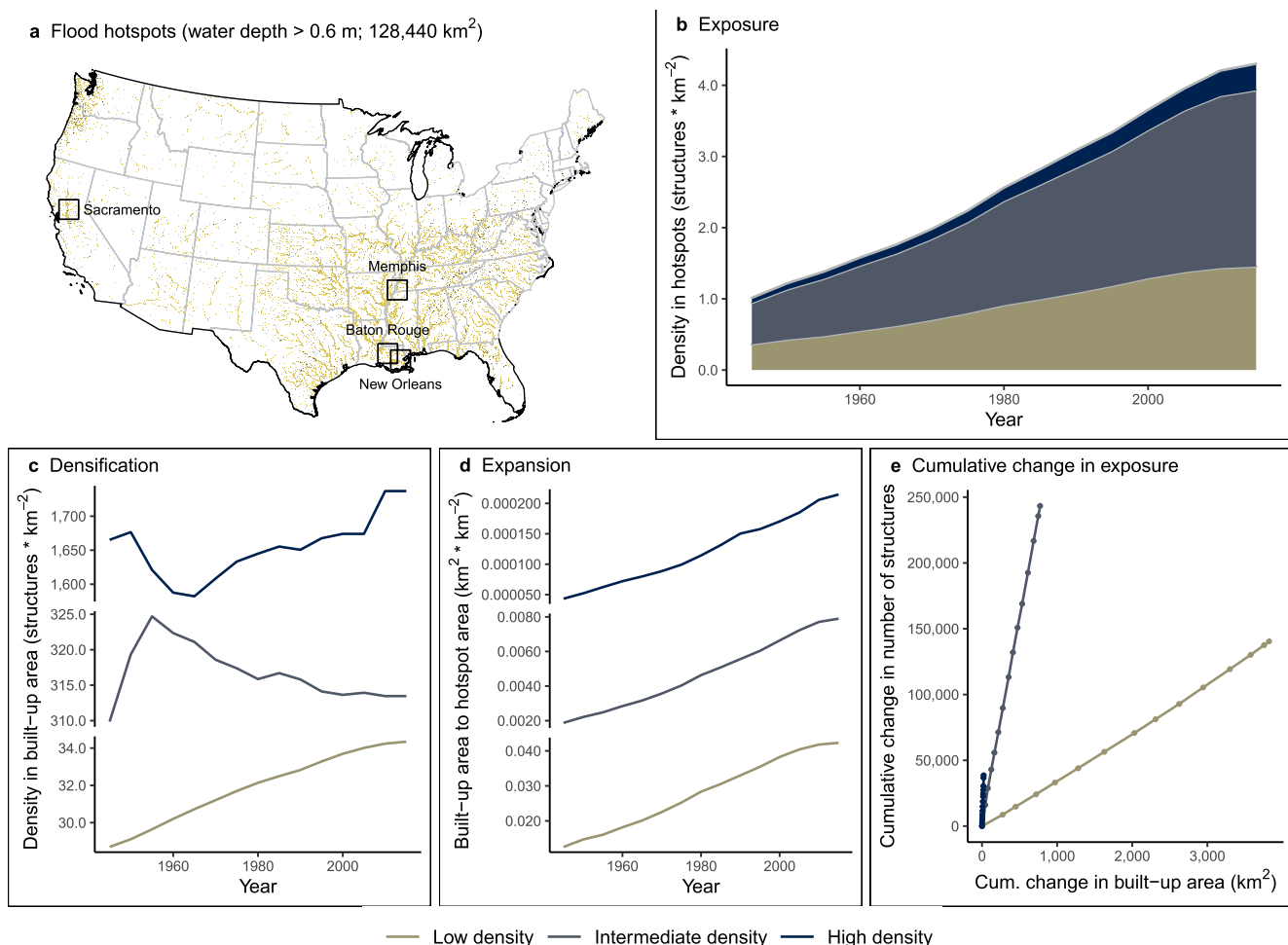


Figure 4. Exposure to floods (1945–2015). Water depth is assumed to be constant over the entire period, and changes in exposure are attributed solely to development. (a) Location of flood hotspots. Temporal trends in (b) exposure, (c) densification, and (d) expansion of structures in the flood hotspots. Note that y-axis scales are different in (c and d). (d) Cumulative changes in the number of structures in flood hotspots as a function of cumulative changes in occupied area. The dots represent years between 1945 and 2015 at 5-year intervals. In all cases, the variables are grouped by classes of development (i.e., low density = 1–112 structures $\times \text{km}^{-2}$; intermediate-density = 113–1,130 structures $\times \text{km}^{-2}$; and high-density $>1,130$ structures $\times \text{km}^{-2}$).

for discussion of the implications of this criterion). The extent of damage to structures of events of these characteristics depends on building type, water depth, flood duration, and speed of the current. Depth-damage curves suggest that structural failure due to static inundation is rare, but a 0.6-m flood would compromise ~30% of a two-story building, including major damage to finishes, contents, and inventory (Pistrika et al., 2014).

Flooding is a local phenomenon. Hotspots have a relatively small total extent ($128,440 \text{ km}^2$) and are home to 552,000 structures, mainly concentrated in intermediate-density areas (Figure 4a). Since 1945, the rate of growth of settlements and towns along rivers and within floodplains has been 30% lower than the national average (Figures 1b and 4b). This pattern likely reflects the expansion of river towns into the surrounding area away from flood hazard (Figures 4c–4e), as well as the establishment of levees and other protective infrastructure. Despite shifts in development toward suburbs and the small geographic extent of the hotspots, floods cause more property damage than any other natural hazard in CONUS (CEMHS, 2019). Urbanization in hazardous areas accounts for part of the increasing losses (Downton et al., 2005). However, 36% of damages in 1988–2017 was attributed to more frequent heavy precipitation, suggesting that climate change may be exacerbating the cost of inundation (Davenport et al., 2021).

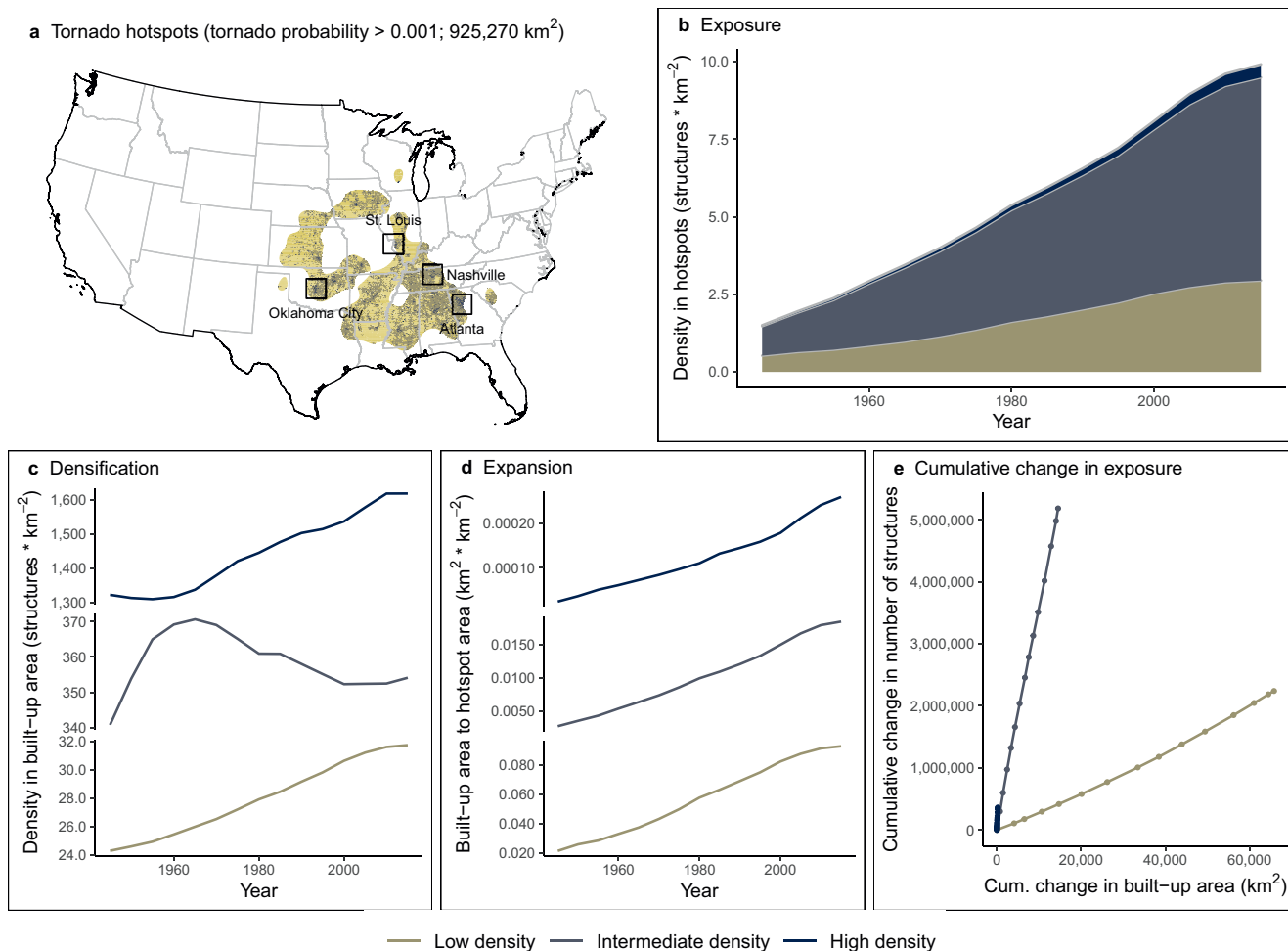


Figure 5. Exposure to tornadoes (1945–2015). Tornado probability is assumed to be constant over the entire period, and changes in exposure are attributed solely to development. (a) Location of tornado hotspots. Temporal trends in (b) exposure, (c) densification, and (d) expansion of structures in the tornado hotspots. Note that y-axis scales are different in (c and d). (e) Cumulative changes in the number of structures in the tornado hotspots as a function of cumulative changes in occupied area. The dots represent years between 1945 and 2015 at 5-year intervals. In all cases, the variables are grouped by classes of development (i.e., low density = 1–112 structures × km⁻²; intermediate-density = 113–1,130 structures × km⁻²; and high-density >1,130 structures × km⁻²).

3.3.2. Tornadoes

Tornadoes are concentrated in the Midwest, south-central US, and Gulf coastal plain (Figure S1d). The spatiotemporal footprint of tornadoes is relatively small, with heavy-tailed duration and path-length distributions. Most tornadoes last less than an hour or two, and travel distances typically on the order of tens of kilometers, although tracks over 300 km long have been reported (Battan, 1959; Johns et al., 2013). Of the ~1,000 tornadoes each year, most occur in late spring through early fall, with longer paths in the southern and central Great Plains (Farney & Dixon, 2015). Extreme winds are the main cause of damage to the built environment from tornadoes.

Tornado hotspots, that is, pixels where the annual probability of at least one tornado is larger than 0.001, represent a 925,270 km² area that largely overlaps with the “Tornado Alley” (Figure 5a). In this region, juxtaposition of large hazard potential and pronounced social and structural vulnerability associated with elevated poverty rates and substantial mobile home densities creates very high risk to lives and property (Ashley & Strader, 2016). Similar to other hazards, the ability to withstand and recover from tornadoes is dependent on social factors. Economically advantaged residents typically prefer to repair or rebuild structures affected by extreme winds rather than relocate. In contrast, socioeconomically vulnerable populations are forcibly mobile, even when disaster declarations and federal aid are in effect (Raker, 2020).

During the last eight decades, structures in tornado hotspots were built at a similar rate as across CONUS (Figures 1b and 5b). Development was historically skewed toward low- and intermediate-density areas, and the long-term increase in exposure to tornadoes can be largely attributed to expansion into less developed lands (Figures 5c–5e). In the 2000's, however, expansion and densification rates in the high-density class up to 1.8 and 2.3 times larger than the national average, respectively, led to a substantial addition of structures to hazardous areas. This increase is a likely consequence of the booming economies of large cities in tornado hotspots, such as Atlanta (impacted by a tornado in May 2008; Coffin, 2008). Were these trends to continue, average tornado impacts in 2100 are expected to be 6 times greater than in 1940 (Strader et al., 2017).

3.3.3. Wildfires

Wildfire hazard potential (WHP) in CONUS is markedly regional (Figure S1e). Wildfire behavior is influenced by socioeconomic and management activities altering fuel load and continuity as well as probability of ignition, with the hazard itself affected by development. Wildfires, in turn, can increase the likelihood of subsequent disturbances, such as landslides or floods, and cause severe air pollution over large areas (Gill & Malamud, 2014).

We defined wildfire hotspots as pixels where WHP is larger than 1,663 (90th percentile of the WHP distribution), meaning that the relative potential for wildfire that would be difficult to suppress is high to very high (Dillon, 2018). Similar to floods, wildfire hotspots are geographically fragmented and less extensive than those delimited for earthquakes and hurricanes (365,880 km²; Figure 6a). Between 1945 and 2015, over 330,000 buildings were added to these fire-prone areas. Although this is the smallest number of structures built among hotspots, it represents an 18-fold increase in density and a 10-fold growth of the exposed built-up area with respect to 1945. Densification and expansion rates in wildfire hotspots are thus three and 10 times higher than the national mean, respectively (Figures 1b–1f and 6b–6e). Analysis of past fires suggests that these estimates are very conservative, as an average of 2.5 million homes, most of which lie in areas of moderate hazard potential, were within or less than 1 km from the boundaries of wildfires every year between 1992 and 2015 (Mietkiewicz et al., 2020).

The addition of new structures to wildfire hotspots was non-linear with a clear inflection point in the mid-1970s (Figure 6b). Increased exposure mainly resulted from the expansion of low- and intermediate-density settlements (Figures 6c–6e), where houses mingle with vegetation. This spatial arrangement further increases wildfire potential by facilitating the introduction of human-related ignitions, which start 84% of fires that threaten homes (Balch et al., 2017), into flammable landscapes. In 2016, the estimated impacts of fire on private property and infrastructure were approximately 60 billion USD (Schoennagel et al., 2017). High-cost, high-loss events like the 2018 Camp Fire in California that resulted in 85 fatalities and damage estimated at 16.5 USD exemplify the rising risk associated with the expansion and proliferation of buildings and ignitions in wildlands, against a backdrop of a warming climate.

Building codes that do not explicitly account for the potential effects of natural hazards allow the proliferation of vulnerable structures. Expansion typically produces more, and more affordable housing than densification (Bitter et al., 2007), and is frequently associated with fewer planning and zoning restrictions than densification (Geshkov & DeSalvo, 2012). Given these considerations, the main implications of exposure predominantly driven by expansion, as observed in flood, tornado, and wildfire hotspots, are twofold. First, risk may rise significantly in years to come due to spread of more vulnerable structures. Second, expansion may increase exposure disproportionately in lower-income or disadvantaged communities. In the future, natural disturbances may therefore meet high property and social vulnerability, resulting in large disruptions to communities, slow recovery, and greater social inequality.

4. Case Study of Flood Exposure and Vulnerability in the Sacramento Valley

Our national scale analysis of exposure focused solely on the development of new structures in hazard zones, thus ignoring other important and hard to quantify elements of risk. For example, human modification of natural systems, both intended and unintended, may confound interpretations of trends in risk. We use this case study to highlight how structure-level data can help address these challenges when impacts are analyzed at the process level and considered in their local social-environmental context. To illustrate this potential, we focus on flooding potential in the Sacramento Valley because it is a large river system (a)

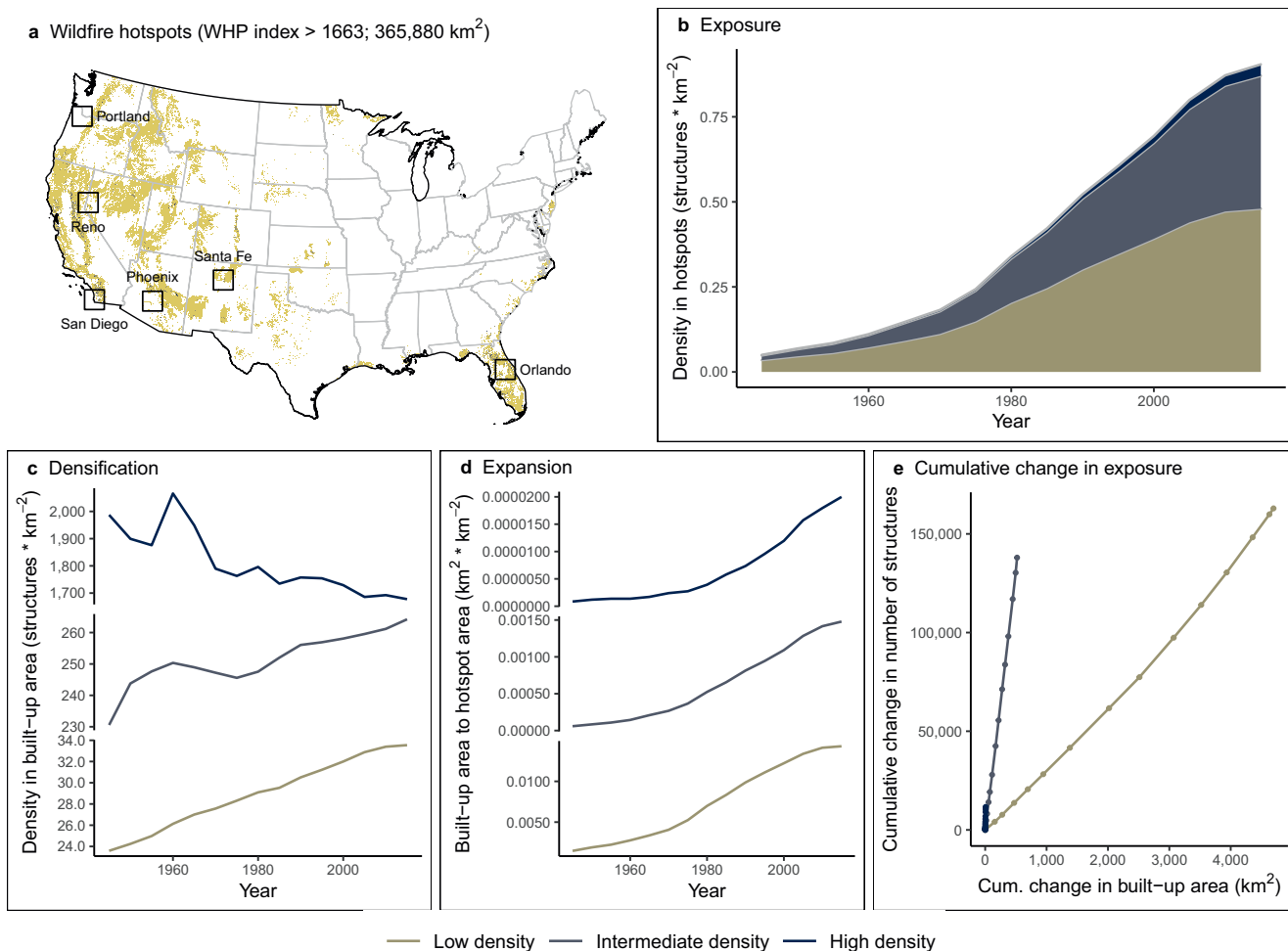


Figure 6. Exposure to wildfires (1945–2015). Wildfire hazard potential is assumed to be constant over the entire period, and changes in exposure are attributed solely to development. (a) Location of wildfire hotspots. Temporal trends in (b) exposure, (c) densification, and (d) expansion of structures in the wildfire hotspots. Note that y-axis scales are different in (c and d). (d) Cumulative changes in the number of structures in the wildfire hotspots as a function of cumulative changes in occupied area. The dots represent years between 1945 and 2015 at 5-year intervals. In all cases, the variables are grouped by classes of development (i.e., low density = 1–112 structures × km⁻²; intermediate-density = 113–1,130 structures × km⁻²; and high-density >1,130 structures × km⁻²).

characterized by high flood hazard, (b) well-suited to the scale of our risk analysis, and (c) extensively protected by levees and water diversions engineered under a regulatory framework.

Early water management efforts in the Sacramento Valley focused on taming the Sacramento River into a single-threaded river using artificial levees. This strategy was at odds with naturally low river conveyance capacities and frequent inundation of the valley (James & Singer, 2008), and further exacerbated by river aggradation that was triggered by hydraulic mining in the Sierra Nevada (Gilbert, 1917). Modern river management began with the Sacramento River Flood Control Project in 1911, which coordinated interventions along the river system using a series of water diversions that established the Sutter and Yolo bypasses (James & Singer, 2008). While still heavily reliant on levees to protect populated areas, keeping water in the Sacramento River itself was no longer a management goal.

The Sacramento-San Joaquin river network is an oft-cited system for the so-called “levee effect” (Di Baldassarre et al., 2015), whereby flood control structures actually increase flood risk (Burton & Cutter, 2008) and alter risk perception, in part, by removing floodplains from federal designations of flood hazard (Ludy & Kondolf, 2012). Decisions on the variables used to communicate hazard and set insurance regulations (e.g., the “100-year floodplain”) may mask residual risk, especially where a hazard at one probability level strongly differs from another. Levees are designed to withstand floods with a certain probability like the

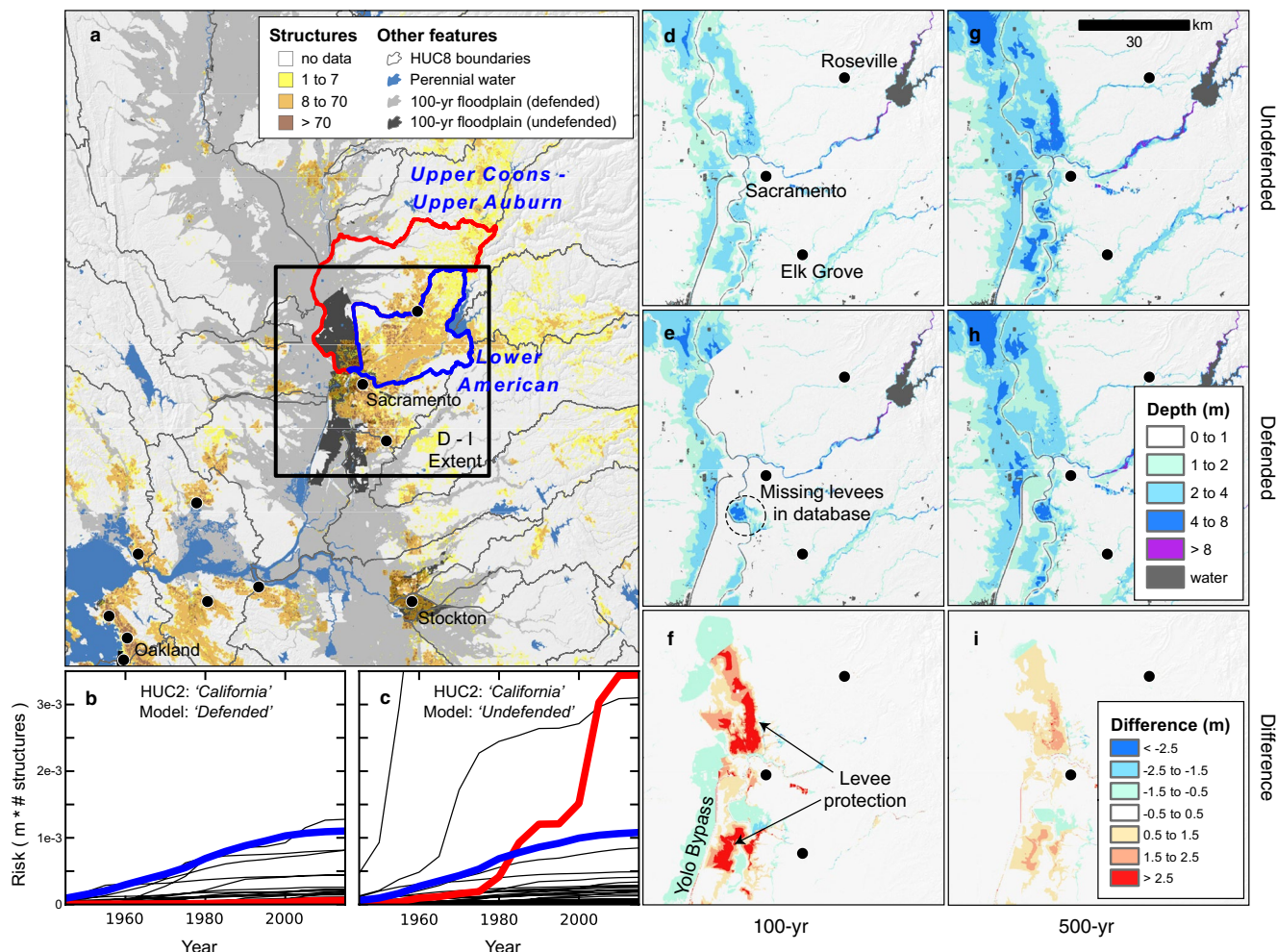


Figure 7. Sacramento River Valley and Sacramento-San Joaquin delta region (California) (a) Site map showing the 100-year floodplain with and without levee protection, Hydrologic Unit Code 8 (HUC8) watershed boundaries, and built-up structure counts for 2015. (b and c) Trends in flood risk (Equation 4) for all HUC8 watersheds in the “California” HUC2 basin for the (b) “defended” and (c) “undefended” models (Sampson et al., 2015; Wing et al., 2017). Colored lines represent the two adjacent HUC8 watersheds highlighted in (a). (d–i) Depth maps for the “100-year” (left column) and “500-year” flood (right column). For each, the top row shows depths from the “undefended” model; the middle row shows depths from the defended model; and the bottom row shows the difference between the two.

100-year flood, but not to reduce the risk of more extreme events (Pinter et al., 2016). This point is illustrated by contrasting inundation depths at different probability levels. Differences between the “defended” and “undefended” model variants (Sampson et al., 2015; Wing et al., 2017) indicate that the protection conferred by levees is dramatically reduced for the 500-year flood (Figure 7) and non-existent for the 1000-year event (Figure S6). “Defended” areas are therefore exposed with a large number of structures potentially experiencing 1–4 m of inundation during the 500-year flood (Figure 7h). Threshold-dependent declines in protection have serious implications, as levee failure and overtopping account for 33% of flood losses in the US (Committee on Risk-Based Analysis for Flood Damage Reduction, 2000). Moreover, climate change may alter the underlying likelihood of river flooding in some areas (Swain et al., 2020; Wobus et al., 2017), and protected communities under historical conditions may no longer be so in the near future.

The challenge of characterizing hazard is not limited to public perceptions of risk, but to any framework where a threshold is used to define exposure to hazards and risk. Our national scale assessment of exposure (previous sections), for instance, accounted for spatial variations in inundation depths by screening for the upper 10% of flood depths. Nevertheless, it still is contingent on choosing a threshold (100-year flood) and a hydrodynamic model (“defended”; Sampson et al., 2015; Wing et al., 2017). While such uniform treatments

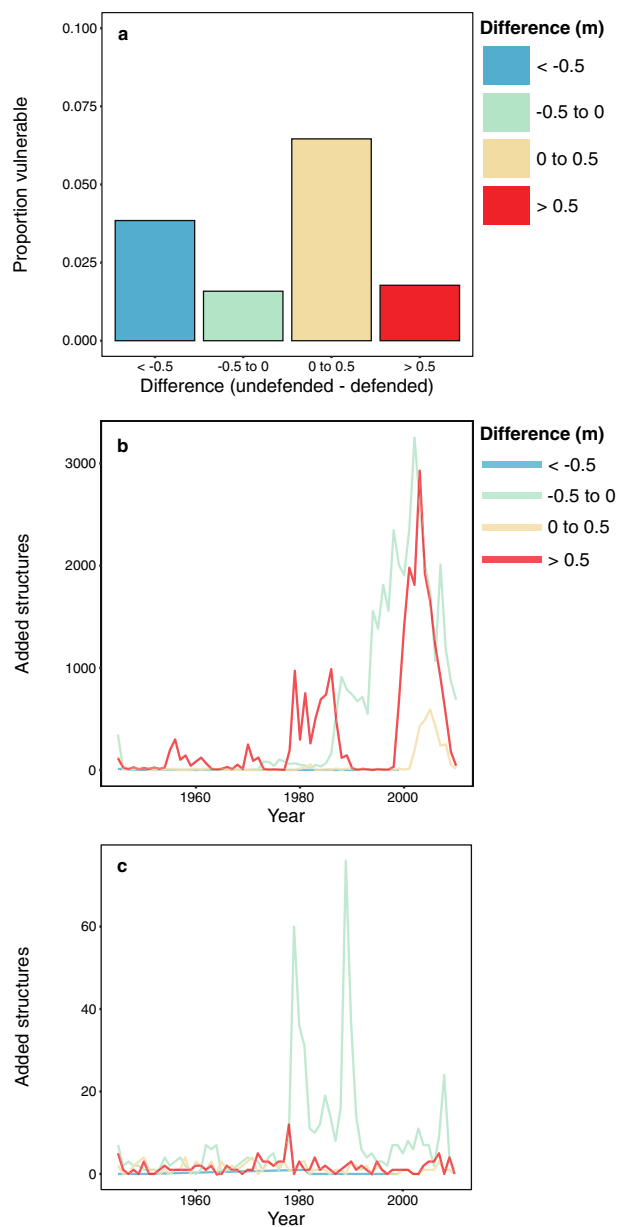


Figure 8. Vulnerable land uses in defended and undefended sectors of the Upper Coons/Upper Auburn watersheds. Levee protection is inferred from differences in the depth of the 100-year flood estimated with the undefended and defended models (see Figure 7). (a) Proportion of vulnerable land uses in undefended (negative/small positive differences; shown in blue, green and yellow) and defended (large positive differences; shown in red). Note that most buildings in the watershed are in places where the models do not differ much. (b) Addition of non-vulnerable and (c) vulnerable structures across inundation classes in 1945–2015 (y-axis scales are different).

are needed and informative to delineate general policies, national scale analyses are not suited to evaluating local risk, with potentially serious implications for decision-makers. The issue is especially evident in the Upper Coons/Upper Auburn watershed (Figure 7a). From our national scale analysis, this watershed appears as a region of very low flood risk because we used the 100-year floodplain that accounts for flood control infrastructure (Figure 7b). However, if we had instead chosen the “undefended” model, accelerated development in the southern portion of the watershed during the late 1980’s and early 2000’s led this area to become the second riskiest in California (Figure 7c), an important implication supported by any risk assessment that considers longer recurrence time floods (Figures 7g–7i and S6).

Development trends for this watershed are dominated by a small area protected by the RD 1000-Natomas earthen levee system, nestled between the confluence of the American and Sacramento Rivers. About a third of the new development in the watershed is in areas where levees afford >0.5 m of protection from inundation (Figure 7). Today, the levee-protected area is home to over 120,000 people, 24,000 structures, and 6 billion USD of assets (National Levee Database; US Army Corps of Engineers). Vulnerable structures, such as low-income housing, hospitals, and schools, represent a very small but important proportion of the total number of buildings within hazardous zones. This ratio is similar in neighboring communities (Figure 8a), suggesting that vulnerable buildings were not preferentially built into or excluded from the sector protected by RD 1000-Natomas.

In defended areas, non-vulnerable structures were added in two main pulses (Figure 8b), a trend that reflects new construction behind levees and the increasing risk shown in Figure 7c. This growth pattern is consistent with the so-called “levee effect.” For example, in neighboring Yuba County to the north, rapid post-levee expansion of homes into floodplains was largely precipitated by population pressure from nearby urban centers along with the removal of required homeowner flood insurance for houses behind the levee (Hutton et al., 2019). In contrast, the slow and relatively constant addition of non-vulnerable structures (Figure 8c) may indicate progressive gentrification driven by the inflated sense of security that levees provide. Given the small number of vulnerable structures built over this time, nonetheless, caution is warranted in over-interpreting trends, or lack thereof, in development of vulnerable structures behind this levee system. While we fully recognize that building type only accounts for one aspect of vulnerability, we emphasize here that the structure-level attributes of the Zillow data provide new opportunities to characterize interactions between vulnerability and historic development patterns in hazard zones. As such, we view this case study as a template for future efforts that can be tailored toward local hazards and incorporate structure-level data, including the estimation of damage functions over multiple hazard probability levels (Pistrikas et al., 2014).

5. Conclusions

Increasing exposure is a key driver of worsening losses from natural hazards. Using unique, fine-scaled data on the built environment, linked to hazards maps for earthquake, flood, hurricane, tornado, and wildfire, we

found that hazard hotspots cover 31% of the country, but 57% of structures are located within their boundaries. A slowing of exposure growth in the last decade reflects the national pattern of economic slowing, yet in all cases the number of structures in hazard hotspots is still growing.

One of the most significant barriers in national scale risk assessments is inadequate characterization of development patterns (Willis et al., 2016). The use of fine-scale data on the built environment provides advances in risk assessment including (a) more accurate identification of exposed structures, (b) detailed information on the characteristics of the places where people live, work and recreate, and (c) assessment of the land development patterns leading to changes in exposure (e.g., expansion and densification). Our results show that, while large in-fill urban and suburban development plays a key role in growing earthquake and hurricane exposure, expansion into previously undeveloped lands especially drives development in flood, tornado and wildfire hotspots. The subtle interactions of hazard geography at the urban-rural fringe particularly affect flood and wildfire exposure. River-side cities are expanding beyond their floodplains, so new suburban settlements tend to be less exposed. Conversely, the growth of relatively low density development into natural vegetation increases wildfire exposure, and injects more human ignitions into flammable landscapes (Balch et al., 2017). This relatively recent, compound phenomenon suggests potential for significant increase in wildfire loss in the near future.

Hazard hotspots analyses with fine-resolution exposure data can also point to where mitigation efforts are most likely to be effective, and how they might best be implemented. For example, regional planning and investment patterns might most affect future hurricane losses, whereas local codes that make buildings safer would pay-off for earthquake and tornado hazards. A mixture of approaches, including micro-zonation and building codes, should be directed at wildfire and flood hotspots. In all cases, care is needed to assess the potential for “levee effects” whereby mitigation actions induce further exposure, vulnerability, or both. As illustrated with the construction of levees in the Sacramento Valley, model assumptions and regulatory frameworks shape the design of mitigation efforts and may inadvertently increase the risk of extreme events. It is worth noting that high risk can exist in other parts of the country where hazard frequency and magnitude is lower but exposure is disproportionately larger due to the concentration of people and assets. Finally, climate change will alter the occurrence and intensity of weather- and climate-related events in ways difficult to predict but with worrisome trends. Growing attention to such trends by financial and insurance firms, in turn, may start to alter development patterns. The dynamic nature of risk makes understanding exposure imperative in this rapidly changing environment.

Acknowledgments

Funding for this work was provided by Earth Lab through the University of Colorado Boulder's Grand Challenge Initiative; NSF's Humans, Disasters, and the Built Environment program (award #1924670 to CU Boulder); and the Innovative Seed Grant program at CU Boulder. This research benefited from support provided to the University of Colorado Population Center (CUPC, Project 2P2CHD066613-06) from the Eunice Kennedy Shriver Institute of Child Health Human and Human Development. The content is solely the responsibility of the authors and does not necessarily represent the official views of NIH or CUPC. The authors gratefully acknowledge access to the Zillow Transaction and Assessment Data set (ZTRAX) through a data use agreement between the University of Colorado Boulder and Zillow Group, Inc. The results and opinions are those of the authors and do not reflect the position of Zillow Group. The authors would like to gratefully acknowledge Fathom for the use of flood modeling products in the manuscript (<https://www.fathom.global/>).

Data Availability Statement

Data sets for this research are available in these citations: Demuth et al. (2006), Dillon (2018), Leyk and Uhl (2018), NOAA (2019), Rukstales and Shumway (2019), Sampson et al. (2015), and Uhl and Leyk (2020). More information on accessing the data can be found at <http://www.zillow.com/ztrax>.

References

- Agee, E., & Childs, S. (2014). Adjustments in tornado counts, F-scale intensity, and path width for assessing significant tornado destruction. *Journal of Applied Meteorology and Climatology*, 53(6), 1494–1505. <https://doi.org/10.1175/JAMC-D-13-0235.1>
- Alig, R. J., Kline, J. D., & Lichtenstein, M. (2004). Urbanization on the US landscape: Looking ahead in the 21st century. *Landscape and Urban Planning*, 69(2–3), 219–234. <https://doi.org/10.1016/j.landurbplan.2003.07.004>
- Anderson, B., Ferreri, J., Al-Hamdan, M., Crosson, W., Schumacher, A., Guikema, S., et al. (2020a). Assessing United States county-level exposure for research on tropical cyclones and human health. *Environmental Health Perspectives*, 128(10), 107009. <https://doi.org/10.1289/EHP6976>
- Anderson, B., Schumacher, A., Guikema, S., Quiring, S., & Ferreri, J. (2020b). *Stormwindmodel: Model tropical cyclone wind speeds (version 0.1.2)*. Retrieved from <https://github.com/geanders/stormwindmodel>
- ASCE. (2014). *Seismic evaluation and retrofit of existing buildings* (41st ed.). American Society of Civil Engineers. <https://doi.org/10.1061/9780784412855>
- Ashley, W. S., & Strader, S. M. (2016). Recipe for disaster: How the dynamic ingredients of risk and exposure are changing the tornado disaster landscape. *Bulletin of the American Meteorological Society*, 97(5), 767–786. <https://doi.org/10.1175/BAMS-D-15-00150.1>
- Balch, J. K., Bradley, B. A., Abatzoglou, J. T., Nagy, R. C., Fusco, E. J., & Mahood, A. L. (2017). Human-started wildfires expand the fire niche across the United States. *Proceedings of the National Academy of Sciences*, 114(11), 2946–2951. <https://doi.org/10.1073/pnas.1617394114>
- Batibeniz, F., Ashfaq, M., Diffenbaugh, N. S., Key, K., Evans, K. J., Turuncoglu, U. U., & Önal, B. (2020). Doubling of U.S. Population exposure to climate extremes by 2050. *Earth's Future*, 8(4). <https://doi.org/10.1029/2019EF001421>
- Battan, L. J. (1959). Duration of tornadoes. *Bulletin of the American Meteorological Society*, 40(7), 340–342. <https://doi.org/10.1175/1520-0477-40.7.340>

- Bitter, C., Mulligan, G. F., & Dall'erba, S. (2007). Incorporating spatial variation in housing attribute prices: A comparison of geographically weighted regression and the spatial expansion method. *Journal of Geographical Systems*, 9(1), 7–27. <https://doi.org/10.1007/s10109-006-0028-7>
- Boschken, H. L. (1982). The demands of conflicting change on public enterprise: West coast seaport development and environmental regulation. *Public Administration Review*, 42(3), 220. <https://doi.org/10.2307/976007>
- Bouwer, L. M. (2011). Have disaster losses increased due to anthropogenic climate change? *Bulletin of the American Meteorological Society*, 92(1), 39–46. <https://doi.org/10.1175/2010BAMS3092.1>
- Burton, C., & Cutter, S. L. (2008). Levee failures and social vulnerability in the Sacramento-San Joaquin Delta area, California. *Natural Hazards Review*, 9(3), 136–149. [https://doi.org/10.1061/\(ASCE\)1527-6988\(2008\)9:3\(136\)](https://doi.org/10.1061/(ASCE)1527-6988(2008)9:3(136))
- CEMHS. (2019). *Spatial hazard events and losses database for the United States (version 18.8)*. Center for Emergency Management and Homeland Security, Arizona State University. Retrieved from <https://sheldus.asu.edu/SHELDUS/>
- Coffin, B. (2008). Atlanta drops the ball during surprise tornado. *Risk Management*, 55(5), 15.
- Committee on Risk-Based Analysis for Flood Damage Reduction. (2000). *Risk analysis and uncertainty in flood damage reduction studies*. National Academy Press.
- Crossett, K. M., Culliton, T. J., Wiley, P. C., & Goodspeed, T. R. (2005). *Population trends along the coastal United States, 1980–2008*.
- Cutter, S. L., Boruff, B. J., & Shirley, W. L. (2003). Social vulnerability to environmental hazards. *Social Science Quarterly*, 84(2), 242–261. <https://doi.org/10.1111/1540-6237.8402002>
- Cutter, S. L., & Emrich, C. (2005). Are natural hazards and disaster losses in the U.S. increasing? *Eos Transactions American Geophysical Union*, 86(41), 381–389. <https://doi.org/10.1029/2005EO410001>
- Cutter, S. L., & Finch, C. (2008). Temporal and spatial changes in social vulnerability to natural hazards. *Proceedings of the National Academy of Sciences*, 105(7), 2301–2306. <https://doi.org/10.1073/pnas.0710375105>
- Cutter, S. L., Hodgson, M. E., & Dow, K. (2001). Subsidized inequities: The spatial patterning of environmental risks and federally assisted housing. *Urban Geography*, 22(1), 29–53. <https://doi.org/10.2747/0272-3638.22.1.29>
- Davenport, F. V., Burke, M., & Diffenbaugh, N. S. (2021). Contribution of historical precipitation change to US flood damages. *Proceedings of the National Academy of Sciences*, 118(4), e2017524118. <https://doi.org/10.1073/pnas.2017524118>
- Davies, I. P., Haugo, R. D., Robertson, J. C., & Levin, P. S. (2018). The unequal vulnerability of communities of color to wildfire. *PLoS One*, 13(11), e0205825. <https://doi.org/10.1371/journal.pone.0205825>
- Demuth, J. L., DeMaria, M., & Knaff, J. A. (2006). Improvement of advanced microwave sounding unit tropical cyclone intensity and size estimation algorithms. *Journal of Applied Meteorology and Climatology*, 45(11), 1573–1581. <https://doi.org/10.1175/JAM2429.1>
- Depietri, Y., & McPhearson, T. (2018). Changing urban risk: 140 years of climatic hazards in New York City. *Climatic Change*, 148(1–2), 95–108. <https://doi.org/10.1007/s10584-018-2194-2>
- Di Baldassarre, G., Viglione, A., Carr, G., Kuil, L., Yan, K., Brandimarte, L., & Blöschl, G. (2015). Debates-Perspectives on socio-hydrology: Capturing feedbacks between physical and social processes. *Water Resources Research*, 51(6), 4770–4781. <https://doi.org/10.1002/2014WR016416>
- Dillon, G. K. (2018). *Wildfire hazard potential (WHP) for the conterminous United States (270-m GRID)* [data set]. Forest Service Research Data Archive. <https://doi.org/10.2737/RDS-2015-0047-2>
- Dixon, P. G., Mercer, A. E., Grala, K., & Cooke, W. H. (2013). Objective identification of tornado seasons and ideal spatial smoothing radii. *Earth Interactions*, 18(2), 1–15. <https://doi.org/10.1175/2013EI000559.1>
- Downton, M. W., Miller, J. Z. B., & Pielke, R. A. (2005). Reanalysis of U.S. National Weather Service Flood Loss Database. *Natural Hazards Review*, 6(1), 13–22. [https://doi.org/10.1061/\(ASCE\)1527-6988\(2005\)6:1\(13\)](https://doi.org/10.1061/(ASCE)1527-6988(2005)6:1(13))
- Ehrlich, D., Melchiorri, M., Florczyk, A., Pesaresi, M., Kemper, T., Corbane, C., et al. (2018). Remote sensing derived built-up area and population density to quantify global exposure to five natural hazards over time. *Remote Sensing*, 10(9), 1378. <https://doi.org/10.3390/rs10091378>
- Elliott, J., & Pais, J. (2010). When nature pushes back: Environmental impact and the spatial redistribution of socially vulnerable populations. *Social Science Quarterly*, 91, 1187–1202. <https://doi.org/10.1111/j.1540-6237.2010.00727.x>
- Emrich, C. T., & Cutter, S. L. (2011). Social vulnerability to climate-sensitive hazards in the southern United States. *Weather, Climate, and Society*, 3(3), 193–208. <https://doi.org/10.1175/2011WCAS1092.1>
- Evans, J. (2018). Tornado warnings in flash flood emergencies: What do we expect people to do? *Bulletin of the American Meteorological Society*, 99(8), 1517.
- Farney, T. J., & Dixon, P. G. (2015). Variability of tornado climatology across the continental United States. *International Journal of Climatology*, 35(10), 2993–3006. <https://doi.org/10.1002/joc.4188>
- FEMA NFIP. (2020). *Federal Insurance & Mitigation Administration National Flood Insurance Program (FIMA NFIP) Redacted Claims Dataset*. Retrieved from <https://www.fema.gov/media-library/assets/documents/180374>
- Formetta, G., & Feyen, L. (2019). Empirical evidence of declining global vulnerability to climate-related hazards. *Global Environmental Change*, 57, 10190. <https://doi.org/10.1016/j.gloenvcha.2019.05.004>
- Fuchs, S., Keiler, M., & Zischg, A. (2015). A spatiotemporal multi-hazard exposure assessment based on property data. *Natural Hazards and Earth System Sciences*, 15(9), 2127–2142. <https://doi.org/10.5194/nhess-15-2127-2015>
- Fuchs, S., Röthlisberger, V., Thaler, T., Zischg, A., & Keiler, M. (2017). Natural hazard management from a coevolutionary perspective: Exposure and policy response in the European Alps. *Annals of the American Association of Geographers*, 107(2), 382–392. <https://doi.org/10.1080/24694452.2016.1235494>
- Gall, M., Borden, K. A., Emrich, C. T., & Cutter, S. L. (2011). The unsustainable trend of natural hazard losses in the United States. *Sustainability*, 3(11), 2157–2181. <https://doi.org/10.3390/su3112157>
- Geshkov, M. V., & DeSalvo, J. S. (2012). The effect of land-use controls on the spatial size of U.S. urbanized areas. *Journal of Regional Science*, 52(4), 648–675. <https://doi.org/10.1111/j.1467-9787.2012.00763.x>
- Gilbert, G. K. (1917). *Hydraulic-mining debris in the Sierra Nevada (First)*. U.S. Government Printing Office.
- Gill, J. C., & Malamud, B. D. (2014). Reviewing and visualizing the interactions of natural hazards. *Reviews of Geophysics*, 52(4), 680–722. <https://doi.org/10.1002/2013RG000445>
- Godschalk, D. R. (2003). Urban hazard mitigation: Creating resilient cities. *Natural Hazards*, 4(3), 136–143. [https://doi.org/10.1061/\(ASCE\)1527-6988\(2003\)4:3\(136\)](https://doi.org/10.1061/(ASCE)1527-6988(2003)4:3(136))
- Gonzalez, R., & Woods, R. (2002). *Digital image processing* (2nd ed.). Prentice-Hall.
- Grimm, N. B., Faeth, S. H., Golubiewski, N. E., Redman, C. L., Wu, J., Bai, X., & Briggs, J. M. (2008). Global change and the ecology of cities. *Science*, 319(5864), 756–760. <https://doi.org/10.1126/science.1150195>

- Hauer, M. E., Evans, J. M., & Mishra, D. R. (2016). Millions projected to be at risk from sea-level rise in the continental United States. *Nature Climate Change*, 6(7), 691–695. <https://doi.org/10.1038/nclimate2961>
- Herring, S. C., Christidis, N., Hoell, A., Hoerling, M. P., & Stott, P. A. (2020). Explaining extreme events of 2018 from a climate perspective. *Bulletin of the American Meteorological Society*, 101(1), S1–S134. <https://doi.org/10.1175/BAMS-ExplainingExtremeEvents2018.1>
- Highfield, W. E., Peacock, W. G., & Van Zandt, S. (2014). Mitigation planning: Why hazard exposure, structural vulnerability, and social vulnerability matter. *Journal of Planning Education and Research*, 34(3), 287–300. <https://doi.org/10.1177/0739456X14531828>
- Hutton, N. S., Tobin, G. A., & Montz, B. E. (2019). The levee effect revisited: Processes and policies enabling development in Yuba County, California. *Journal of Flood Risk Management*, 12(3), e12469. <https://doi.org/10.1111/jfr3.12469>
- IPCC. (2007). *Climate change 2007. Synthesis report: Contribution of Working Groups I, II, and III to the fourth assessment report of the Intergovernmental Panel on Climate Change*. Cambridge University Press. Retrieved from <http://www.ipcc.ch/pdf/assessment-report/ar4/wg2/ar4-wg2-ts.pdf>
- IPCC. (2012). *Managing the risks of extreme events and disasters to advance climate change adaptation. A special report of Working Groups I and II of the Intergovernmental Panel on Climate Change*. Cambridge University Press.
- Jaiswal, K., Bausch, D., Rozelle, J., Holub, J., & McGowan, S. (2017). Hazus estimated annualized earthquake losses for the United States (Federal Government Series No. FEMA P-366) (p. 75). Federal Emergency Management Agency. Retrieved from <https://pubs.er.usgs.gov/publication/70189832>
- James, A. L., & Singer, M. B. (2008). Development of the lower Sacramento Valley flood-control system: Historical perspective. *Natural Hazards Review*, 9(3), 125–135. [https://doi.org/10.1061/\(ASCE\)1527-6988\(2008\)9:3\(125\)](https://doi.org/10.1061/(ASCE)1527-6988(2008)9:3(125))
- Johns, R. H., Burgess, D. W., Iii, C. A. D., Gilmore, M. S., Hart, J. A., & Piltz, S. F. (2013). The 1925 tri-state tornado damage path and associated storm system (Vol. 33). <https://doi.org/10.1353/ner.2013.0020>
- Latif, M., Keenlyside, N., & Bader, J. (2007). Tropical sea surface temperature, vertical wind shear, and hurricane development. *Geophysical Research Letters*, 34(1), L01710. <https://doi.org/10.1029/2006GL027969>
- Leyk, S., & Uhl, J. (2018). HISDAC-US, historical settlement data compilation for the conterminous United States over 200 years. *Scientific Data*, 5(1), 180175. <https://doi.org/10.1038/sdata.2018.175>
- Leyk, S., Uhl, J., Connor, A., Baswell, A., Mietkiewicz, N., Balch, J., & Gutmann, M. (2020). Two centuries of settlement and urban development in the United States. *Science Advances*, 6(23), eaba2937. <https://doi.org/10.1126/sciadv.eaba2937>
- Ludy, J., & Kondolf, G. M. (2012). Flood risk perception in lands “protected” by 100-year levees. *Natural Hazards*, 61(2), 829–842. <https://doi.org/10.1007/s11069-011-0072-6>
- Lyles, L. W., Berke, P., & Smith, G. (2014). Do planners matter? Examining factors driving incorporation of land use approaches into hazard mitigation plans. *Journal of Environmental Planning and Management*, 57(5), 792–811. <https://doi.org/10.1080/09640568.2013.768973>
- Ma, C., & Smith, T. (2020). Vulnerability of renters and low-income households to storm damage: Evidence from Hurricane Maria in Puerto Rico. *American Journal of Public Health*, 110(2), 196–202. <https://doi.org/10.2105/AJPH.2019.305438>
- Mietkiewicz, N., Balch, J., Schoennagel, T., Leyk, S., StDenis, L., & Bradley, B. (2020). In the line of fire: Consequences of human-ignited wildfires to homes in the U.S. (1992–2015). *Fire*, 3(3), 50. <https://doi.org/10.3390/fire3030050>
- NOAA. (2019). *Storm prediction center severe report database*. Retrieved from <https://www.spc.noaa.gov/wcm/>
- O'Connor, J. E., & Costa, J. E. (2004). Spatial distribution of the largest rainfall-runoff floods from basins between 2.6 and 26,000 km² in the United States and Puerto Rico. *Water Resources Research*, 40(1). <https://doi.org/10.1029/2003WR002247>
- Pais, J., & Elliott, J. (2008). Places as recovery machines: Vulnerability and neighborhood change after major hurricanes. *Social Forces*, 86, 1415–1451. <https://doi.org/10.1353/sof.0.0047>
- Paprotny, D., Morales-Nápoles, O., & Jonkman, S. N. (2018). HANZE: A pan-European database of exposure to natural hazards and damaging historical floods since 1870. *Earth System Science Data*, 10(1), 565–581. <https://doi.org/10.5194/essd-10-565-2018>
- Petal, M. (2004). *Urban disaster mitigation and preparedness: The 1999 Kocaeli earthquake*. University of California.
- Petersen, M. D., Shumway, A. M., Powers, P. M., Mueller, C. S., Moschetti, M. P., Frankel, A. D., et al. (2020). The 2018 update of the US National Seismic Hazard Model: Overview of model and implications. *Earthquake Spectra*, 36(1), 5–41. <https://doi.org/10.1177/8755293019878199>
- Pinter, N., Huthoff, F., Dierauer, J., Remo, J. W. F., & Damptz, A. (2016). Modeling residual flood risk behind levees, Upper Mississippi River, USA. *Environmental Science & Policy*, 58, 131–140. <https://doi.org/10.1016/j.envsci.2016.01.003>
- Pistrikia, A., Tsakiris, G., & Nalbantis, I. (2014). Flood depth-damage functions for built environment. *Environmental Processes*, 1(4), 553–572. <https://doi.org/10.1007/s40710-014-0038-2>
- Raker, E. J. (2020). Natural hazards, disasters, and demographic change: The case of severe tornadoes in the United States, 1980–2010. *Demography*, 57(2), 653–674. <https://doi.org/10.1007/s13524-020-00862-y>
- Rappaport, E. N. (2014). Fatalities in the United States from Atlantic tropical cyclones: New data and interpretation. *Bulletin of the American Meteorological Society*, 95(3), 341–346. <https://doi.org/10.1175/BAMS-D-12-00074.1>
- Ratcliffe, M., Burd, C., Holder, K., & Fields, A. (2016). *Defining rural at the US Census Bureau (American Community Survey and Geography Brief No. ASCGEO-1)*. US Census Bureau. Retrieved from https://www2.census.gov/geo/pdfs/reference/ua/Defining_Rural.pdf
- Reidmiller, D. R., Avery, C. W., Easterling, D. R., Kunkel, K. E., Lewis, K. L. M., Maycock, T. K., & Stewart, B. C. (2018). *Impacts, risks, and adaptation in the United States: The fourth national climate assessment* (Vol. 2). U.S. Global Change Research Program. <https://doi.org/10.7930/NCA4.2018>
- Risser, M. D., & Wehner, M. F. (2017). Attributable human-induced changes in the likelihood and magnitude of the observed extreme precipitation during Hurricane Harvey. *Geophysical Research Letters*, 44(24), 457–512. <https://doi.org/10.1002/2017GL075888>
- Rukstales, K. S., & Shumway, A. M. (2019). *Data release for 2018 update of the U.S. National Seismic Hazard Model* [Data set]. U.S. Geological Survey. <https://doi.org/10.5066/P9WT5OVB>
- Sampson, C. C., Smith, A. M., Bates, P. D., Neal, J. C., Alfieri, L., & Freer, J. E. (2015). A high-resolution global flood hazard model. *Water Resources Research*, 51(9), 7358–7381. <https://doi.org/10.1002/2015WR016954>
- Schoennagel, T., Balch, J. K., Brenkert-Smith, H., Dennison, P. E., Harvey, B. J., Krawchuk, M. A., et al. (2017). Adapt to more wildfire in western North American forests as climate changes. *Proceedings of the National Academy of Sciences*, 114(18), 4582–4590. <https://doi.org/10.1073/pnas.1617464114>
- Schlutz, J., & Elliott, J. (2013). Natural disasters and local demographic change in the United States. *Population and Environment*, 34, 293–312. <https://doi.org/10.1007/s11111-012-0171-7>
- Schumacher, I., & Strobl, E. (2011). Economic development and losses due to natural disasters: The role of hazard exposure. *Ecological Economics*, 72, 97–105. <https://doi.org/10.1016/j.ecolecon.2011.09.002>

- Sebastian, A. G., Lendering, K. T., Kothuis, B. L. M., Brand, A. D., Jonkman, S. N., van Gelder, P. H. A. J. M., et al. (2007). *Hurricane Harvey Report: A fact-finding effort in the direct aftermath of Hurricane Harvey in the Greater Houston Region*. Delft University Publishers.
- Segal, E., Negev, M., Feitelson, E., & Zaychik, D. (2017). Devising 'policy packages' for seismic retrofitting of residences. *Natural Hazards*, 89(1), 497–519. <https://doi.org/10.1007/s11069-017-2978-0>
- Short, K. C. (2017). *Spatial wildfire occurrence data for the United States, 1992–2015* [Data set]. Forest Service Research Data Archive. <https://doi.org/10.2737/RDS-2013-0009>
- Short, K. C., Finney, M. A., Scott, J. H., Gilbertson-Day, J. W., & Grenfell, I. C. (2016). *Spatial dataset of probabilistic wildfire risk components for the conterminous United States* [Data set]. Forest Service Research Data Archive. <https://doi.org/10.2737/RDS-2016-0034>
- Smit, B., & Wandel, J. (2006). Adaptation, adaptive capacity and vulnerability. *Global Environmental Change*, 16(3), 282–292. <https://doi.org/10.1016/j.gloenvcha.2006.03.008>
- Smith, J. H., Wickham, J. D., Stehman, S. V., & Yang, L. (2002). Impacts of patch size and land-cover heterogeneity on thematic image classification accuracy. *Photogrammetric Engineering and Remote Sensing*, 68(1), 65–70.
- Steeves, P., & Douglas, N. (1994). *1:250,000-scale hydrologic units of the United States*. U.S. Geological Survey. Retrieved from <https://water.usgs.gov/GIS/huc.html>
- Strader, S. M., Ashley, W. S., Pingel, T. J., & Krmenev, A. J. (2017). Observed and projected changes in United states tornado exposure. *Weather, Climate, and Society*, 9(2), 109–123. <https://doi.org/10.1175/WCAS-D-16-0041.1>
- SVRGIS. (2019). *Tornado path data*. Retrieved from <https://www.spc.noaa.gov/gis/svrgis/zipped/1950-2018-torn-aspAth.zip>
- Swain, D. L., Wing, O. E. J., Bates, P. D., Done, J. M., Johnson, K. A., & Cameron, D. R. (2020). Increased flood exposure due to climate change and population growth in the United States. *Earth's Future*, 8(11). <https://doi.org/10.1029/2020EF001778>
- Tucker, B. (2007). Trends in global urban earthquake risk: A call to the international Earth Science and Earthquake Engineering communities. *Seismological Research Letters*, 75(6), 695–700.
- Turner, B. L., Kasperson, R. E., Matson, P. A., McCarthy, J. J., Corell, R. W., Christensen, L., et al. (2003). A framework for vulnerability analysis in sustainability science. *Proceedings of the National Academy of Sciences*, 100(14), 8074–8079. <https://doi.org/10.1073/pnas.1231335100>
- Uhl, J., & Leyk, S. (2020). *Fine-grained gridded built-up property statistics for the US over 200 years*. Retrieved from <https://doi.org/10.7910/DVN/YSWMDR>
- Vogel, C., & O'Brien, K. (2004). *Vulnerability and global environmental change: Rhetoric and reality*. Global Environmental Change and Human Security Project.
- Weinkle, J., Landsea, C., Collins, D., Musulin, R., Crompton, R. P., Klotzbach, P. J., & Pielke, R. (2018). Normalized hurricane damage in the continental United States 1900–2017. *Nature Sustainability*, 1(12), 808–813. <https://doi.org/10.1038/s41893-018-0165-2>
- White, G., Kates, R., & Burton, I. (2001). Knowing better and losing even more: The use of knowledge in hazards management. *Global Environmental Change Part B: Environmental Hazards*, 3(3–4), 81–92. [https://doi.org/10.1016/S1464-2867\(01\)00021-3](https://doi.org/10.1016/S1464-2867(01)00021-3)
- Wickham, J. D., Stehman, S. V., Gass, L., Dewitz, J., Fry, J. A., & Wade, T. G. (2013). Accuracy assessment of NLCD 2006 land cover and impervious surface. *Remote Sensing of Environment*, 130, 294–304. <https://doi.org/10.1016/j.rse.2012.12.001>
- Willis, H. H., Narayanan, A., Fischbach, J. R., Molina-Perez, E., Stelzner, C., Loa, K., & Kendrick, L. (2016). *Current and future exposure of infrastructure in the United States to natural hazards*. RAND Corporation. <https://doi.org/10.7249/RR1453>
- Willoughby, H. E. (2012). Distributions and trends of death and destruction from hurricanes in the United States, 1900–2008. *Natural Hazards Review*, 13(1), 57–64. [https://doi.org/10.1061/\(ASCE\)NH.1527-6996.0000046](https://doi.org/10.1061/(ASCE)NH.1527-6996.0000046)
- Wilson, M. J., Sugg, M. M., & Lane, S. J. (2019). Identifying multivariate vulnerability of nursing home facilities throughout the southeastern United States. *International Journal of Disaster Risk Reduction*, 36, 101106. <https://doi.org/10.1016/j.ijdrr.2019.101106>
- Wing, O. E. J., Bates, P. D., Sampson, C. C., Smith, A. M., Johnson, K. A., & Erickson, T. A. (2017). Validation of a 30 m resolution flood hazard model of the conterminous United States. *Water Resources Research*, 53(9), 7968–7986. <https://doi.org/10.1002/2017WR020917>
- Wobus, C., Gutmann, E., Jones, R., Rissing, M., Mizukami, N., Lorie, M., et al. (2017). Climate change impacts on flood risk and asset damages within mapped 100-year floodplains of the contiguous United States. *Natural Hazards and Earth System Sciences*, 17(12), 2199–2211. <https://doi.org/10.5194/nhess-17-2199-2017>
- Worden, C. B. (2016). *ShakeMap manual*. U.S. Geological Survey. <https://doi.org/10.5066/F7D21VPQ>
- Zhou, Y., & Matyas, C. J. (2017). Spatial characteristics of storm-total rainfall swaths associated with tropical cyclones over the Eastern United States. *International Journal of Climatology*, 37, 557–569. <https://doi.org/10.1002/joc.5021>